

Dalton Transactions

Accepted Manuscript



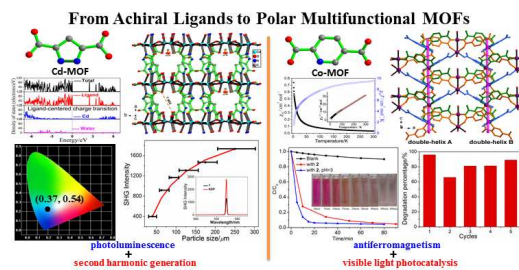
This is an *Accepted Manuscript*, which has been through the Royal Society of Chemistry peer review process and has been accepted for publication.

Accepted Manuscripts are published online shortly after acceptance, before technical editing, formatting and proof reading. Using this free service, authors can make their results available to the community, in citable form, before we publish the edited article. We will replace this *Accepted Manuscript* with the edited and formatted *Advance Article* as soon as it is available.

You can find more information about *Accepted Manuscripts* in the [Information for Authors](#).

Please note that technical editing may introduce minor changes to the text and/or graphics, which may alter content. The journal's standard [Terms & Conditions](#) and the [Ethical guidelines](#) still apply. In no event shall the Royal Society of Chemistry be held responsible for any errors or omissions in this *Accepted Manuscript* or any consequences arising from the use of any information it contains.

Graphical Abstract



Here we report the structures and multiple properties of two polar MOFs, which feature the combined properties of photoluminescence and second harmonic generation for Cd-MOF, and antiferromagnetism and visible light photocatalysis for Co-MOF.

ARTICLE

Structures and multiple properties of two polar metal-organic frameworks based on achiral N,O-coordinated ligands: toward multifunctional materials†

Cite this: DOI: 10.1039/x0xx00000x

Guang-Ning Liu,^{*,a} Ming-Jian Zhang,^b Wan-Qing Liu,^a Hui Sun,^a Xin-Yu Li,^a Ke Li,^a Cai-Ze Ren,^a Zhen-Wei Zhang,^a and Cuncheng Li^{*,a}

Two novel metal-organic frameworks (MOFs) $[\text{Cd}_3(\text{padc})(\text{Hpadc})(\text{H}_2\text{padc})(\text{H}_2\text{O})]_n \cdot n\text{H}_2\text{O}$ (**1**, H_3padc = pyrazole-3,5-dicarboxylic acid) and $[\text{Co}_4(\text{pidc})_2(\text{Hpidc})_4(\text{H}_2\text{O})_3]_n \cdot 12n\text{H}_2\text{O}$ (**2**, H_2pidc = pyridine-2,5-dicarboxylic acid) that both crystallize in polar space groups, were solvothermally synthesized by using achiral N,O-coordinated ligands. Compound **1** consists of trinuclear Cd(II)-based units that are further bridged by the backbone of H_3padc ligands to form a three-dimensional (3-D) (4,6)-connected fsc topology network, while **2** features two types of double-helical tubes with different chiralities connecting with each other alternatively to construct a typical 2-D (3,6)-connected kgd topology network. Importantly, **1** exhibits combined properties of photoluminescence (PL) and second harmonic generation (SHG), and represents the first noncentrosymmetric H_3padc -based MOF that was obtained without any ancillary ligands. While, **2** shows strong antiferromagnetic interaction between paramagnetic Co(II) centers, and the aqueous solution of **2** exhibits effective homogeneous photocatalysis property under visible irradiation. Further, the mechanisms of the physical properties for **1** and **2** were discussed in detail.

Received 00th January 2015,
Accepted 00th January 2015

DOI: 10.1039/x0xx00000x

www.rsc.org/

1. Introduction

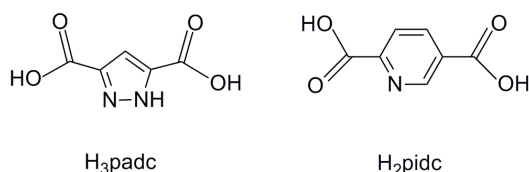
The need for new materials that possess not only one expected property e.g., mechanical, electronic, optical, catalytic, separation and magnetic properties, but also combine two or more of them in a single compound is continuously increasing.¹ Metal-organic frameworks (MOFs) featuring superiorities in rational design and synthesis have become a research hotspot in multifunctional material field.² Several considerable merits guarantee MOFs are one of the best candidates during the exploration of multifunctional materials. Firstly, the combination of metal ions with flexible organic ligands via coordination bonds (also known as a combination of inorganic and organic species) in a single MOF can lead to the coexistence or synergism of the properties from both types of constituents e.g., the magnetism or catalysis properties originated from metal ions, and the optical property derived from organic ligands.³ Secondly, applying some strategies e.g., modifying the structure or the morphology of MOFs, can endow MOFs with additional properties except those that were closely related to the nature of the metal ions or the organic ligands. For example, it is known that control synthesis of MOFs with cavities in different radii could induce additional properties, like storage,⁴ separation,⁵ ion exchange (or dye exchange),⁶ drug delivery⁷ and as a stabilizer for catalysis.⁸ Also, the reduction of MOF crystals to nanoscale⁹ or fabricating

MOF film¹⁰ can give rise to properties discrepant from the microcrystalline samples that are most frequently obtained through the wet solution chemistry or the solvo(hydro)thermal methods. Finally, post-synthetic modification or in-situ synthesis of MOFs with functional species encapsulated in the cavities has recently emerged as an effective tool for constructing multifunctional MOFs.¹¹

Besides the above mentioned effective strategies, another important strategy to enrich the property of MOFs is to synthesize noncentrosymmetric (NCS) structures.¹² It is known that NCS structures have some proprietary functions e.g., second harmonic generation (SHG) and ferroelectricity (that is more strictly to require the material to crystallize in NCS space groups belonging to the ten polar point groups). Undoubtedly, the construction of MOFs that crystallize in NCS structure, even polar structure is very helpful for the exploration of multifunctional materials. Nevertheless, the practicable and effective strategies to construct NCS materials are under developing, it is still a big challenge to synthesize NCS or polar MOFs, especially for the utilization of achiral organic ligands.¹³

Recently, our attention has been focused on the preparation of NCS structures. By utilizing polar chalcogenidometalate anion or chiral dinuclear metal complex as a building unit or as a template, we have already synthesized several interesting NCS compounds with multiple properties.¹⁴ In order to further explore this work, we aim to synthesize NCS

multifunctional MOFs by using achiral organic ligands, which are more plentiful and easier to synthesize than chiral ligands. The selection of two achiral N,O-coordinated ligands, pyrazole-3,5-dicarboxylic acid ($H_3\text{padc}$, Scheme 1) and pyridine-2,5-dicarboxylic acid ($H_2\text{pidc}$, Scheme 1) each respectively to react with d^{10} Cd(II) metal ion or paramagnetic Co(II) metal ion affords two polar MOFs, namely $[\text{Cd}_3(\text{padc})(\text{Hpadc})(\text{H}_2\text{padc})(\text{H}_2\text{O})]_n \cdot n\text{H}_2\text{O}$ (**1**) and $[\text{Co}_4(\text{pidc})_2(\text{Hpidc})_4(\text{H}_2\text{O})_3]_n \cdot 12n\text{H}_2\text{O}$ (**2**). Apart from the intriguing crystal structures of both compounds, **1** exhibits multiple properties of PL and SHG response, while **2** exhibits strong antiferromagnetic behavior and effective photocatalysis property under visible irradiation. Herein, we report the syntheses, crystal structures and multiple properties of **1** and **2**. Furthermore, the mechanisms of the properties of **1** and **2** are discussed in detail.



Scheme 1 The achiral ligands used to construct polar MOFs in this work.

2. Experimental section

2.1 Materials and characterization

All reagents were purchased commercially and used without further purification. Elemental analyses of C, H, and N were performed on an Elementar Vario EL III microanalyzer. Powder X-ray diffraction (PXRD) patterns were recorded on Bruker D8 Focus diffractometer using $\text{Cu } K\alpha$ radiation. A Perkin-Elmer Diamond thermogravimetric analyzer was used to obtain thermogravimetric analyses (TGA) curves in N_2 with a flow rate of 20 mL/min and a ramp rate of $10\text{ }^\circ\text{C}\cdot\text{min}^{-1}$ in the temperature range 30–900 $^\circ\text{C}$. An empty Al_2O_3 crucible was used as the reference. The FT-IR spectra were recorded on a Perkin-Elmer spectrophotometer using KBr disk in the range 4000–400 cm^{-1} . Optical diffuse reflectance spectra were measured at room temperature with a Shimadzu UV-310 PC UV/Vis spectrophotometer. The instrument was equipped with an integrating sphere and controlled with a personal computer. The samples were ground into fine powder and pressed onto a thin glass slide holder where BaSO_4 plate was used as a standard (100% reflectance). The absorption spectra were calculated from reflectance spectrum using the Kubelka-Munk function:¹⁵ $\alpha/S = (1-R)^2/2R$ where α is the absorption coefficient, S is the scattering coefficient (which is practically wavelength independent when the particle size is larger than 5 μm), and R is the reflectance.

2.2 FL and NLO experiments

The solid-state fluorescence excitation and emission spectra were measured on an Edinberg EI920 fluorescence spectrophotometer at room temperature with a wavelength increment of 1.0 nm and integration time of 0.2 s. Powder SHG measurement of **1** was performed on a modified Kurtz-NLO system using 1.064 μm laser radiation. The SHG signal was collected and focused into a fiber optic bundle. The output of the fiber optic bundle was coupled to the entrance slit of a spectrometer and detected using a CCD detector. KDP powder

was used as a reference to assume the second-order nonlinear optical (NLO) effect. SHG efficiency has been shown to depend strongly on particle size, thus samples of KDP as well as **1** were ground and sieved into several distinct particle size ranges (30–50, 50–75, 75–100, 100–150, 150–200, 200–300 μm).

2.3 Computational details

The X-ray crystallographic data of **1** was used to calculate its electronic structure. The calculation of density of states (DOS) was carried out using density functional theory (DFT) with one of the three nonlocal gradient-corrected exchange-correlation functionals (GGA-PBE) and performed with the CASTEP code¹⁶, which uses a plane wave basis set for the valence electrons and norm-conserving pseudopotential for the core electrons¹⁷. The number of plane waves included in the basis was determined by a cutoff energy, E_c , of 340 eV. Pseudo-atomic calculations were performed for Cd $4d^{10}5s^2$, O $2s^22p^4$, C, $2s^22p^2$, N $2s^22p^3$ and H $1s^1$. The parameters used in the calculations and convergence criteria were set by the default values of the CASTEP code¹⁶.

2.4 Photocatalytic and Magnetic experiments

The evaluation of photocatalytic activity of **2** for the photocatalytic decolorization of organic dyes was performed at ambient temperature. The procedure was as follows: 0.020 g of powder sample was dissolved in 40 mL water and then 0.2 mL of 2.0×10^3 mg/L Rhodamine B (RhB) aqueous solution was added (with final concentration of 10.0 mg L^{-1}). Five drops of hydrogen peroxide solution (H_2O_2 , 30%) were added and the pH value was adjusted to 3 with sulfuric acid (H_2SO_4 , 0.5 mol/L). A 300 W xenon arc lamp fitted with an optical filter was used as a light source. The optical filter was used to filter out the UV emission below 400 nm so as to irradiate the sample with only visible light. During the degradation, the mixture was stirred continuously by means of a magnetic stirrer. At different time intervals, analytical samples were withdrawn and analyzed by UV/Vis spectroscopy. The polycrystalline magnetic study of **2** was performed on a Quantum Design PPMS-9T magnetometer. All data was corrected for diamagnetism estimated from Pascal's constants.

2.5 Preparations of 1–2

2.5.1 Preparation of 1. A mixture of $H_3\text{padc}$ (0.048 g, 0.30 mmol), $\text{CdCl}_2 \cdot 2.5\text{H}_2\text{O}$ (0.069 g, 0.30 mmol), $\text{H}_2\text{C}_2\text{O}_4 \cdot 2\text{H}_2\text{O}$ (0.018 g, 0.14 mmol), acetonitrile (2.0 mL) and distilled water (2.0 mL) was sealed in a 25-mL poly(tetrafluoroethylene)-lined stainless steel container under autogenous pressure and then heated at 150 $^\circ\text{C}$ for 5 days and finally cooled to room temperature. Colorless chip crystals of **1** were obtained and washed with ethanol. (Yield: 88% based on Cd). Elemental analysis: calcd. (%) for $\text{C}_{15}\text{H}_{10}\text{Cd}_3\text{N}_6\text{O}_{14}$: C 21.56, H 1.21, N 10.06; found: C 21.62, H 1.66, N 10.65. IR (KBr pellet, cm^{-1}) 3634(vw), 3483(m), 3131(s), 3059(s), 2955(s), 2867(s), 2815(w), 2701(w), 2530(vw), 2250(w), 1623(m), 1551(s), 1509(w), 1442(m), 1364(vs), 1209(m), 1105(wv), 1053(m), 1022(s), 846(s), 784(s), 633(w), 546(m), 520(m).

2.5.2 Preparation of 2. A mixture of $H_2\text{pidc}$ (0.033 g, 0.20 mmol), $\text{Co}(\text{NO}_3)_2 \cdot 6\text{H}_2\text{O}$ (0.058 g, 0.30 mmol), acetonitrile (6.0 mL) and distilled water (4.0 mL) was sealed in a 25-mL poly(tetrafluoroethylene)-lined stainless steel container under

autogenous pressure and then heated at 130 °C for 5 days and finally cooled to room temperature. Purple flaky crystals of **2** occurred together with yellow prismatic crystals of a known compound $[\text{Co}_2(\text{picd})_2(\text{H}_2\text{O})_6]n \cdot 2n\text{H}_2\text{O}$ ¹⁸ in the product. The attempts to obtain pure phase of **2** were unsuccessful. Compound **2** was manually separated and washed with ethanol and diethyl ether. (Yield: 41% based on Co). Elemental analysis: calcd. (%) for $\text{C}_{42}\text{H}_{52}\text{Co}_4\text{N}_6\text{O}_{39}$: C 33.62, H 3.49, N 5.60; found: C 33.09, H 3.52, N 5.51. IR (KBr pellet, cm^{-1}) 3421(s), 2924(vw), 2851(vw), 1665(vs), 1623(s), 1483(w), 1400(vs), 1328(s), 1276(m), 1167(w), 1116(vw), 1053(w), 835(m), 769(m), 733(w), 680(w), 536(m).

For **1**, it should be noted that although oxalic acid does not indwell the final structure, it is indispensable in the preparation of **1**; otherwise, a known compound was obtained instead.¹⁹ Most likely, the oxalic acid may regulate the acidity of the reaction system that finally influence the coordination mode of the organic ligands.

Compound **1** is insoluble in common solvents, while compound **2** is soluble in water. The phase purities of crystals of **1** and **2** for physical property measurements were confirmed by PXRD studies (Fig. S1). The experimental PXRD patterns are in good agreement with the simulated patterns from the single-crystal structures, which reveals the phase purity of the bulk crystalline materials.

2.6 Single-crystal structure determination

The intensity data sets of **1** and **2** were collected on a Agilent Xcalibur, Eos, Gemini CCD diffractometer equipped with a graphite-monochromated Mo $K\alpha$ radiation ($\lambda = 0.71073 \text{ \AA}$) at 77 K. The data sets were reduced by the CrysAlisPro²⁰ program. An empirical absorption correction using spherical harmonics was implemented in SCALE3 ABSPACK scaling algorithm. The structures were solved by direct methods using the Siemens SHELXL package of crystallographic software.²¹ Difference Fourier maps were created on the basis of these atomic positions to yield the other non-hydrogen atoms. The structures were refined using a full-matrix least-squares refinement on F^2 . All non-hydrogen atoms were refined anisotropically. For charge neutralization, it is suggested that the carboxyl of part ligands in **1** and **2** are not deprotonated completely but exists as H_2padc^- in **1** and Hpicd^- in **2**. The protons were located near O23 in **1**, and O21 and O33 in **2** from a Difference Fourier synthesis. Further, from the Difference Fourier map of **2**, a number of diffuse scattered peaks with electron density were observed in the 1-D channels, which can be attributed to the disordered water molecules. PLATON/SQUEEZE was used to refine the structure further.²² The molecular formula of **2** was calculated and confirmed by the elemental analysis data and thermogravimetric analyses. The hydrogen atoms of water molecules in **1** and the coordinated water molecules in **2** were located by Difference Fourier map and refined with O–H distances to a target value of 0.85 Å and $U_{\text{iso}}(\text{H}) = 1.5U_{\text{eq}}(\text{O})$. The hydrogen atoms of the lattice water molecules in **2** were not added. The hydrogen atoms on the

pyrazole ring of **1** and the pyridine ring of **2** were located at geometrically calculated positions and refined as riding on their parent atoms with fixed isotropic displacement parameters [$U_{\text{iso}}(\text{H}) = 1.2U_{\text{eq}}(\text{C}, \text{N})$]. Crystallographic data and structural refinements for **1–2** are summarized in Table 1. Important bond lengths and angles are listed in Table S1.

Table 1. Crystal and Structure Refinement Data for **1–2**.

	1	2
Formula	$\text{C}_{15}\text{H}_{10}\text{Cd}_3\text{N}_6\text{O}_{14}$	$\text{C}_{42}\text{H}_{52}\text{Co}_4\text{N}_6\text{O}_{39}$
M_r (g mol^{-1})	835.49	1500.62
Crystal system	Monoclinic	Orthorhombic
Space group	Pc (Polar)	$\text{Cmc}2_1$ (Polar)
Flack factor	−0.04(4)	0.01(2)
ρ_{calcd} [g cm^{-3}]	2.042	1.680
a [Å]	8.8438(7)	25.7987(12)
b [Å]	12.7821(9)	23.5734(12)
c [Å]	12.2085(8)	9.7527(5)
α [°]	90	90
β [°]	100.063(7)	90
γ [°]	90	90
V [Å ³]	1358.85(17)	5931.2(5)
Z	2	4
T [K]	77(2)	77(2)
$F(000)$	796	3064
θ range [°]	3.19–25.50	3.14–25.50
Measured reflections	6818	5502
Independent reflections (R_{int})	4417 (0.0300)	5502 (0.0000)
Data/parameters/restraints	4235/358/9	4505/421/24
R_1^a, wR_2^b [$I > 2\sigma(I)$]	0.0357, 0.0926	0.0523, 0.1278
Goodness of fit	1.002	1.005
$\Delta\rho_{\text{max}}$ and $\Delta\rho_{\text{min}}$ [e \AA^{-3}]	1.097, −0.525	0.546, −0.472

$$^a R_1 = \sum ||F_o| - |F_c|| / \sum |F_o|, \quad ^b wR_2 = \{ \sum w[(F_o)^2 - (F_c)^2]^2 / \sum w(F_o)^2 \}^{1/2}$$

3. Results and discussion

3.1 Crystal structures

3.1.1 Crystal structure of 1. Single-crystal X-ray diffraction analysis reveals that compound **1** crystallizes in the monoclinic noncentrosymmetric and polar space group Pc , and features a 3-D structure constructed by Cd(II) ions, backbones of H_3pada ligands, and water molecules. Each asymmetric unit of **1** contains three Cd(II) ions, three deprotonated H_3pada ligands, one coordinated water molecule and one lattice water molecule (Fig. 1). The three crystallographically independent Cd(II) ions adopt three types of coordination geometries. The Cd1 atom is six-coordinated by four carboxylate O atoms and two pyrazole N atoms to produce a distorted ($\text{Cd}1\text{O}_4\text{N}_2$) octahedral coordination environment.²³ While the Cd2 and Cd3 atoms each is seven-coordinated to form a distorted pentagonal bipyramid: the former is surrounded by five carboxylate O atoms and two pyrazole N atoms to form a ($\text{Cd}2\text{O}_5\text{N}_2$) polyhedron; the latter is surrounded by six carboxylate O atoms and one water O atom to form a ($\text{Cd}3\text{O}_7$) polyhedron (Fig. S4). Both Cd–N and Cd–O bond lengths are well within their normal ranges.²⁴ The H_3pada ligand in **1** employs three types:²⁵ mono-deprotonated H_2padc^- , di-deprotonated Hpadc^{2-} , and fully deprotonated padc^{3-} , which exhibit different coordination modes (Fig. S5). Both Hpadc^{2-} and H_2padc^- adopt a tridentate mode, specifically $\mu_3\text{-}\kappa\text{O}11, \text{O}12$: $\kappa\text{O}12, \text{N}11$: $\kappa\text{O}13$ mode for Hpadc^{2-} to link two symmetry-

related Cd1 centers and one Cd3 center, and μ_3 - κ O21, O22: κ O22, N21: κ O23 mode for H_2padc^{2-} to link two symmetry-related Cd2 centers and one Cd3 center. The $padc^{3-}$ ligand adopts a pentadentate mode μ_5 - κ O31,O32: κ O32, N31: κ N32, O34: κ O33, O34: κ O33 to link two symmetry-related Cd1, two symmetry-related Cd2, and one Cd3 center. The $(Cd_2O_5N_2)$ and (Cd_3O_7) pentagonal bipyramids, and $(Cd_1O_4N_2)$ octahedra connecting with each other to form trinuclear $[Cd_3]$ units, which are further linked by μ_5 - $padc^{3-}$ ligands to form a 2-D hybrid layer parallel to the bc plane (Fig. S6). The μ_3 - H_2padc^- and μ_3 - $Hpadc^{2-}$ ligands acting as pillars connect the 2-D hybrid layer to form a 3-D framework with lattice water molecules reside in the 1-D channels along the c direction (Fig. 2a). There are also O–H...O and N–H...O hydrogen bonds within the 3-D framework of **1** (Fig. S7, Table S2).

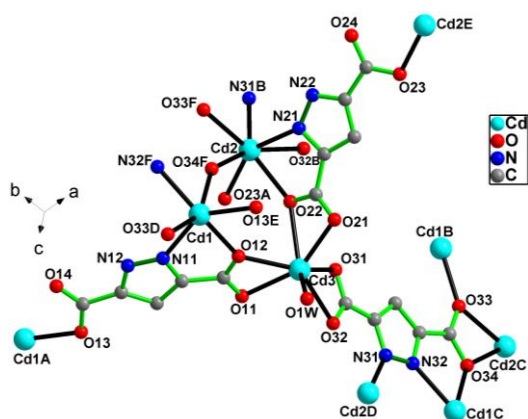


Fig. 1 The coordination environments around Cd^{2+} ions in **1**. Symmetry codes: A $(-1+x, y, z)$; B $(x, 1-y, -0.5+z)$; C $(x, -1+y, z)$; D $(x, 1-y, 0.5+z)$; E $(1+x, y, z)$; F $(x, 1+y, z)$.

From a topological point of view, if the trinuclear $[Cd_3]$ unit and the μ_5 - $padc^{3-}$ ligand were all treated as a 4-connected node, the 2-D hybrid layer parallel to the bc plane is a typical 4-connected 2-D framework with a sql topology network (Fig. 2b). Taking into consideration the μ_3 - H_2padc^- and μ_3 - $Hpadc^{2-}$ ligands as linkers bridging the hybrid 2-D layers, a 3-D (4,6)-connected fsc topology network with a point symbol of $\{4^4.6^{10}.8\}\{4^4.6^2\}$ can be rationalized by TOPOS 4.0 for **1** (Fig. 2c).²⁶ It should be noted that although nearly one hundred metal-organic coordination compounds with deprotonated H_3pada ligands have been reported, most of them crystallize in centric structures or crystallize in NCS structure but with the collaboration of ancillary ligands.²⁷ To our knowledge, compound **1** represents the first NCS MOF based on H_3pada ligand but without any ancillary ligands.

3.1.2 Crystal structure of 2. Compound **2** crystallizes in the orthorhombic noncentrosymmetric and polar space group Cmc_21 , and contains 2-D $[Co_4(pidc)_2(Hpidc)_4(H_2O)_3]$ layers and lattice water molecules. The asymmetric unit of **2** contains two Co(II) ions, one $pidc^{2-}$ ligand, two $Hpidc^-$ ligands, 1.5 coordinated water molecules and six lattice water molecules (Fig. 3). Each Co(II) center is six-coordinated with the coordin-

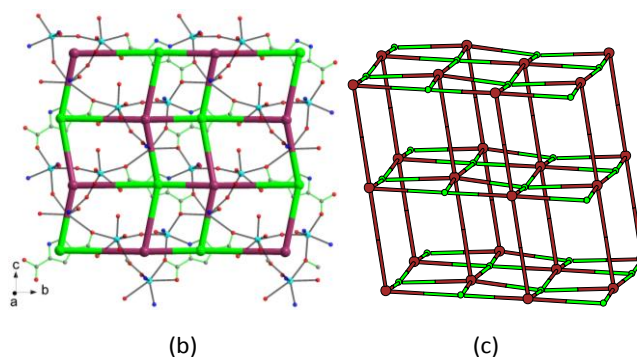
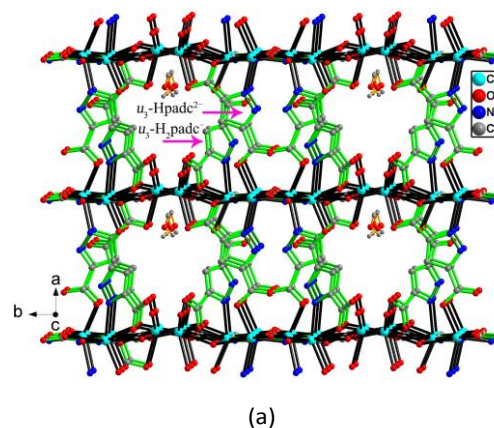


Fig. 2 (a) The 3-D structure of **1** with 1-D channels along the c direction. (b) The topology analysis of the 2-D layer parallel to the bc plane. (c) The schematic representation of **1** (purple color node for $[Cd_3]$ unit, light green node for μ_5 - $padc^{3-}$ ligand).

ation geometry described as a distorted octahedron.²² The Co1 atom is coordinated by one chelating $pidc^{2-}$ and two chelating $Hpidc^-$ ligands in a N,O-chelated mode to form a (CoN_4O_4) octahedron. The Co2 and Co3 atoms are each surrounded by four carboxylate O atoms from two $pidc^{2-}$ and two $Hpidc^-$ ligands, one terminal water molecule, and one bridging water molecule to form a $[Co_2O_{11}]$ dimer with Co...Co distance of 3.595(1) Å. The three crystallographically independent ligands in **2** (denoted as L_{N11} , L_{N21} , and L_{N31}) adopt two types of coordination modes (Fig. S8). L_{N11} employs the fully deprotonated type $pidc^{2-}$ and adopts a tridentate coordination mode, μ_3 - κ O12, N11: κ O13: κ O14. While both L_{N21} and L_{N31} employ the mono-deprotonated type $Hpidc^-$ and adopt bidentate coordination modes (μ_2 - κ O21, N21: κ O24 for the former and μ_2 - κ O32, N31: κ O34 for the later). In **2**, all the deprotonated H_2pidc ligands acting as linkers connect Co1 atoms and $[Co_2]$ dimers in an alternative fashion along the 2_1 screw axis in the $[001]$ direction to form two types of double-helical tubes with opposite chirality (Fig. 4a). Detailed structural analysis suggests that the double-helical tube can be considered to be formed by the weaving of two single helixes showing reverse helical orientation through sharing Co3 atoms (Figs. 5 and S9).²⁸ The pitch of the helical tube along the c direction is the same as the length of the c axis, and the separation between adjacent helical tubes is half of the length of the a axis. The double-helical tubes with different chiralities connect with each

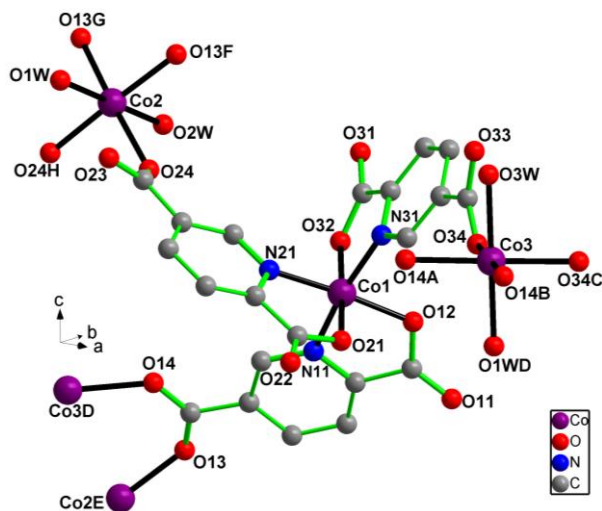


Fig. 3 The coordination environments around Co^{2+} ions in **2**. Symmetry codes: A (1/2-x, 3/2-y, 0.5+z); B (1/2+x, 3/2-y, 0.5+z); C (1-x, y, z); D (1/2-x, 3/2-y, -0.5+z); E (x, y, -1+z); F (x, y, 1+z); G (-x, y, 1+z); H (-x, y, z).

other via sharing the $[\text{Co}_2]$ nodes and alternatively to construct an achiral 2-D $[\text{Co}_4(\text{picd})_2(\text{Hpdc})_4(\text{H}_2\text{O})_3]_n$ layer (Fig. 4a).

Topologically, while the $[\text{Co}_2]$ dimer is simplified as a 6-connected node, and the Co1 atom as a 3-connected node, compound **2** is a typical 2-D (3,6)-connected kgd topology network with a point symbol of $\{4^3\}_2\{4^6\cdot 6^6\cdot 8^3\}$ (Fig. 4b). Such layers are packed along the b direction and form 1-D channels which accommodate the lattice water molecules (Fig. S10). In double-helical tubes, the shortest $\text{Co1}\cdots\text{Co2}$ distance of 7.471(1) Å and the shortest $\text{Co1}\cdots\text{Co3}$ distance of 7.344(1) Å are both significantly longer than the $\text{Co2}\cdots\text{Co3}$ distance in the $[\text{Co}_2]$ dimer (Fig. S11). This is significantly responsible for the magnetic property, as discussed in detail later. Besides the O-H \cdots O hydrogen bonds within the 2-D layer, there are also plenty of O-H \cdots O hydrogen bond interactions between the 2-D layers and the lattice water molecules, which lead to the formation of a 3-D supramolecular framework of **2** (Table S3, Fig. S12).

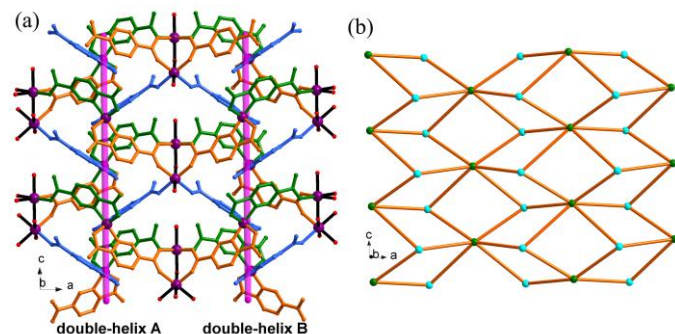


Fig. 4 (a) The 2-D layer structure of **2** constructed from the linkage of L_{N11} (Orange), L_{N21} (Light blue), L_{N31} (Green), and $\text{Co}(\text{II})$ ions (Purple) showing the double-helix tubes. (b) The schematic representation of the layer structure of **2** (turquoise color node for Co1 atom, green node for dimeric $[\text{Co}_2]$ unit).

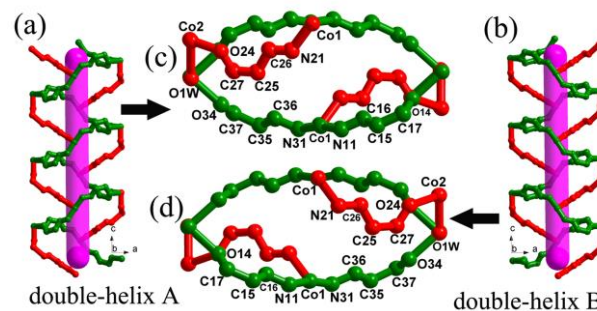


Fig. 5 (a, b) View of the two types of double-helix tubes with different chiralities formed by the weaving of two helices with reverse helical orientation. The pyridine rings and the uncoordinated carboxylate O atoms are omitted for clarity. (c, d) View of the two types of double-helix tubes along the c direction.

3.2 The multiple properties study of **1** and **2**

To explore the multiple properties of the two polar MOFs **1** and **2**, several physical property measurements e.g., the PL for **1**, second-order nonlinear optical (NLO), magnetism (for **2**), photocatalysis were carried out, which were discussed in detail below. Besides, the differential scanning calorimetry measurements (DSC, with the aim to check phase transition behavior that was closely related with the ferroelectric property) in the temperature range of 220–330 K were performed, however no obvious heat anomalies was observed in the DSC curves, which suggested that no phase transition behavior occur for **1** and **2**.

3.2.1 PL property of 1. Photoluminescent d^{10} metal coordination compounds have attracted intensive research interests stemming from their potential applications in chemical sensor, photochemistry and electroluminescent display, etc.²⁹ Here, considering that compound **1** was based on the d^{10} metal ion Cd(II), its solid-state PL property was investigated at room temperature. The solid-state emission and excitation spectra for **1**, together with the Commission Internationale de l'Éclairage (CIE) chromaticity coordinates are shown in Fig. 6. For comparison with the emission spectra of **1**, the solid-state emission spectra of the free H_3padc ligand was also illustrated. Upon irradiation of ultraviolet light at 295 nm, the emission peak of **1** with maxima at 440 nm falls in the region of blue, which is reflected in the CIE chromaticity coordinates (Fig. 6b), exactly in the greenish blue region with a value of (0.20, 0.22). In contrast to the free H_3padc ligand that displays a yellow green emission with maxima around 542 nm and CIE coordinates of (0.37, 0.54), compound **1** shows an obvious fluorescent blue-shift emission.

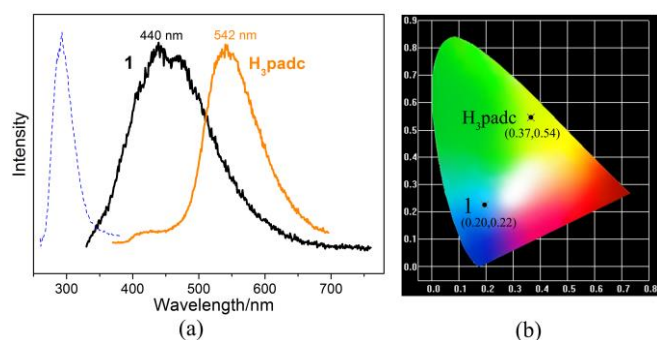


Fig. 6 (a) Solid state emission spectra for **1** (solid black line) and free H₃padc ligand (solid orange line), and solid state excitation spectra of **1** (dashed blue line). (b) The CIE chromaticity diagram for **1** and free H₃padc ligand.

In order to make clear the PL mechanism, theoretical calculation on the single crystal structure by evaluation of the density of states (DOS) was performed. It can be seen from the total and partial DOS diagram (Fig. 7), Cd(II) ion as well as the water molecule make nearly no contribution to the bottom of the conduction bands (CBs) and to the top of the valence bands (VBs), which suggests both of them are not involved in the charge transitions in **1**. On the contrary, the organic ligand constitutes almost entirely to the CBs and VBs, which demonstrates that the ligand-centered charge transition should be responsible for the PL emission of **1**. Compound **1** is insoluble in most common solvents e.g., ethanol, chloroform, acetone, acetonitrile and water, and its emission band falls in the range of the visible light as well as its excitation UV light are commercial available. Compound **1** could be used as potential blue luminescent material for solid-state lighting devices.

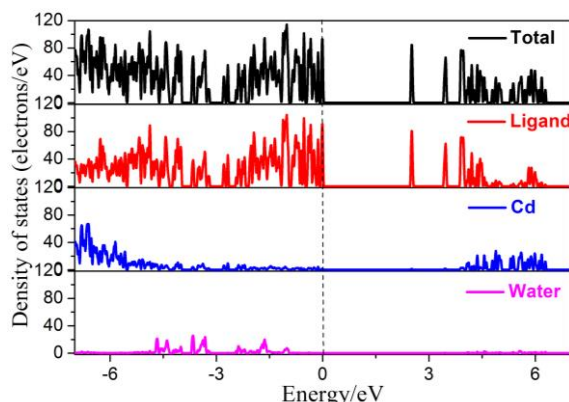


Fig. 7 Total and partial density of states of **1**.

3.2.2 The NLO property of 1. Increasing attention has been focused on the design and synthesis of second-order NLO materials with large SHG efficiency due to their potential and practical applications in the laser industry and optoelectronic technologies.^{13b} Recently, MOFs has become a research hotspot in the realm of SHG materials.^{13a,30} Herein, given that compound **1** crystallizes in NCS space group *Pc*, its second-order NLO effect was investigated. Powder SHG measurement under 1064 nm radiation indicates that compound **1** is SHG active with a response being about 0.5 times as strong as that of

KDP (KH₂PO₄) with the same particle size of 100–150 μm (Fig. 8, Insert). Fig.8 shows that the powder SHG intensity of **1** rises with the increase of the particle size from 30 to 300 μm, and this trend is to continue. It is a typical curve of the type-I phase-matchable material, which is a necessary characteristic for an NLO material to serve for laser frequency conversion.³¹

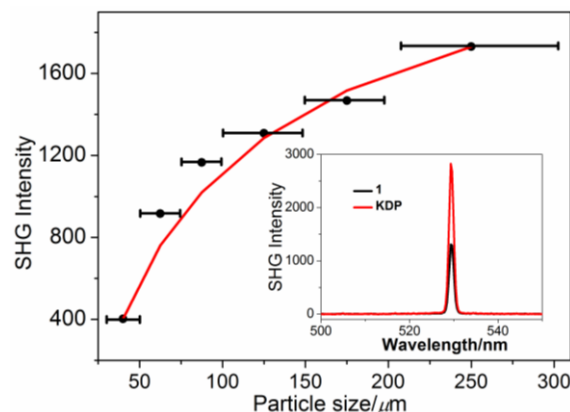


Fig. 8 Phase matching curve (SHG intensity versus particle size) for **1**. Insert: SHG responses of **1** (black) and KDP (red) at 1.064 μm.

Up to now, the NCS MOF based on symmetric ligand with the largest SHG efficiency was known for a Zn-compound, namely [Zn(BPHY)(SA)]_n (BPHY = 1,2-bis(4-pyridyl)-hydrazine, H₂SA = succinic acid), which has a response 11.5 times that of KDP.^{13b} It is well-known that the SHG property is greatly affected by the size and the orientation of the dipole moment of the SHG-active units in the acentric structure. In order to make clear the lower SHG efficiency of **1** compared with [Zn(BPHY)(SA)]_n, an analysis on the size and orientation of the SHG-active units in **1** were carried out. Based on the structural data, the NLO behavior of **1** should be mainly originated from the cooperation of the polarizations of the polar units, including distorted (CdIO₄N₂), (Cd₂O₅N₂) and (Cd₃O₇) polyhedra, and deprotonated H₃padc ligands. For deprotonated H₃padc ligands, the pyrazolyl exhibits as an electron-donating group for the carboxyl that is an electron-accepting group. Meanwhile, the coordination of a carboxyl group to a Cd(II) center leads to the O atom donating a lone pair electrons to the Cd(II) center, which gives rise to another D-A system. Thus, the orientation of the dipole moment of the organic ligand was assigned as shown in Fig. 9. The dipole moment of the Cd-centered polyhedra in the asymmetric unit of **1** and the Zn-centered polyhedron in [Zn(BPHY)(SA)]_n are calculated using a bond-valence approach proposed by Poeppelmerier et al (Table S4). It can be seen that the dipole moments of the Cd-centered polyhedra in the asymmetric unit of **1** are nearly half of that of the Zn-centered polyhedron in [Zn(BPHY)(SA)]_n. Furthermore, the spatial arrangements of the SHG-active units in the unit cell of **1** were not in complete alignment being against the enhancement of macroscopic polarizabilities (Fig. 9), which is significantly different from the nearly paralleled arrangement of the SHG-active units in [Zn(BPHY)(SA)]_n.^{13b} Clearly, all these are responsible for the lower SHG efficiency

of **1** compared with the known NCS compound [Zn(BPHY)(S A)]_n.

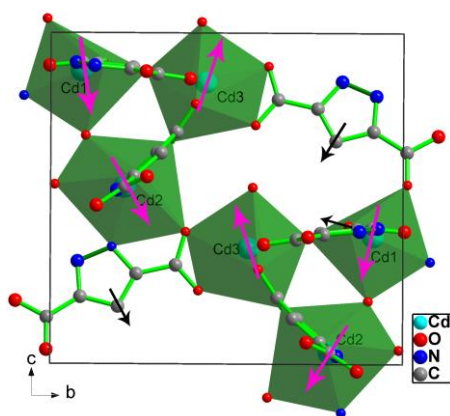


Fig. 9 The dipole moment directions of the polar units in the unit cell of **1**. Pink and black arrows represent the dipoles of Cd-centered polyhedra and the organic ligands, respectively.

In addition, the SHG measurement was also carried out for the compound **2** as it crystallizes in an NCS space group *Cmc2₁*. The powdery sample of **2** was irradiated with 1064 nm laser light; however, no SHG response was observed, which is ascribed to its significant absorption near the SHG wavelength (Fig. S13). Although the result is abjective, it strongly suggests that an effective SHG material should has nearly no absorption in the laser and the SHG wavelength. This is very helpful for us in the further design synthesis of SHG active multifunctional materials.

3.2.3 The magnetic property of 2. The variable-temperature magnetic susceptibility data were collected for polycrystalline sample of **2** at an applied dc field of 1000 Oe in the 2–300 K temperature range. The $\chi_M T$ vs T and χ_M vs T plots for **2** are shown in Fig. 10 (χ_M is the molar magnetic susceptibility per formula). The $\chi_M T$ value of $9.544 \text{ cm}^3 \cdot \text{K} \cdot \text{mol}^{-1}$ at 300 K is significantly larger than the expected value of $7.52 \text{ cm}^3 \cdot \text{K} \cdot \text{mol}^{-1}$ for four high-spin Co(II) ion with $S = 3/2$ and $g = 2.00$, which is typical for high spin Co(II) ions with the significant orbital contribution to the magnetic moment.³² Upon cooling, $\chi_M T$ decreases smoothly until ~ 25 K and then goes down quickly to a minimum value of $1.471 \text{ cm}^3 \cdot \text{K} \cdot \text{mol}^{-1}$ at 2 K, which is related to the depopulation of higher-energy spin-orbit levels of six-coordinated Co(II) centers and antiferromagnetic coupling between Co(II) centers.³³ Meanwhile, χ_M increases gradually from $0.032 \text{ cm}^3 \cdot \text{mol}^{-1}$ at 300 K to a value of $0.739 \text{ cm}^3 \cdot \text{mol}^{-1}$ at about 2 K. The $1/\chi_M$ vs T curve above 75 K obeys the Curie-Weiss law $1/\chi_M = (T - \theta)/C$ with $C = 10.72 \text{ cm}^3 \cdot \text{K} \cdot \text{mol}^{-1}$ and $\theta = -37.90 \text{ K}$ (Fig. 10, insert). The C value is larger than the corresponding value for four high spin-only Co(II) center, suggesting the obvious orbital contribution of the Co(II) center. The negative θ value indicates an overall antiferromagnetic interaction between the Co(II) ions and/or the spin-orbit coupling through the 4T_g state of the octahedral Co(II) ions.

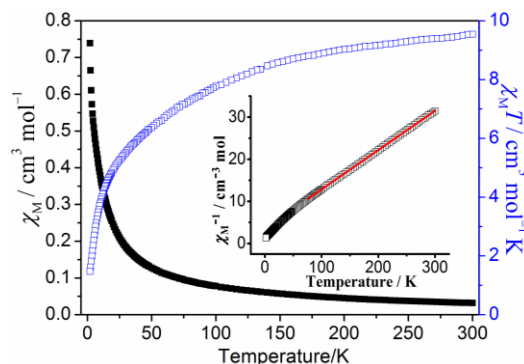


Fig. 10 Temperature dependence of χ_M and $\chi_M T$ for **2**. Insert: the temperature dependence of $1/\chi_M$ for **2** with the solid line representing the fit of the Curie-Weiss law.

The examination of the structure suggests that the Co...Co distance in the [Co₂] dimer of 3.595(1) Å is significantly shorter than the smallest Co...Co separations of 6.972 (1) Å between [Co₂] dimers, 7.231 (1) Å between Co1 ions, and 7.344 (1) Å between [Co₂] dimers and Co1 ions. According to the Goodenough-Kanamori rules, the strongest magnetic interaction are probably within the [Co₂] dimer, where two Co(II) ions are bridged by the carboxyl bridges (Co-OCO-Co) and μ_2 -OH₂ water bridge.^{32b,34} The magnetic exchange angle $\angle \text{Co-O}_{\text{aq}}\text{-Co}$ of $114.12(20)^\circ$ is significantly larger than 90° and close to 120° , which generally leads to strong antiferromagnetic interaction.^{32b,34} This is also verified by the observed very negative Weiss temperature of -37.90 K . On the other hand, the magnetic interaction between dinuclear [Co₂] units and Co1 ions, the interaction between dinuclear [Co₂] units, as well as the interaction between Co1 ions could be weakly antiferromagnetic. The lack of an appropriate magnetic model to describe the magnetic system here has precluded quantitative magnetic analysis for **2**.

3.2.4 Visible light photocatalytic degradation of organic dye of 2. Environmental pollution is one of the major problems that threaten the existence of terrestrial lives,³⁵ and the sunlight provides the most abundant renewable energy source to meet mankind's future energy needs.³⁶ Based on this situation, the utilization of new visible light catalysts has become a hot research topic in the related research community. Recently, a new emerging application of MOFs, photocatalytic degradation of organic pollutants, has been reported.³⁷⁻³⁸ However, most of the reported MOFs in this regard were used as heterogeneous photocatalysts, MOFs used as homogeneous photocatalysts in aqueous solution were rarely reported. Considering that compound **2** is soluble in water (Fig. S16a) and has significant absorption in the visible light region (Fig. S13), it may use as homogeneous photocatalysts for dye wastewater treatment under visible irradiation. Rhodamine B (RhB) was selected as a model dye contaminant to evaluate the photocatalytic efficiency of compound **2** in the degradation of waste water.

Fig. 11 illustrates the time-dependent UV/Vis spectra of dye solution with **2** as photocatalyst. For comparison, the photodegradation process of the organic dye solution without

photocatalyst **2** has also been studied under the same condition. Clearly, the change in the concentration of dye solution is obvious with the use of **2** as a photocatalyst. The characteristic absorption at 553 nm for RhB was selected to monitor its photocatalytic degradation process. As shown in Fig. 11, a rapid degradation of the organic dye solution occurred in the first 30 min, and then the degradation process become slower. It can be seen that the degradation ratio of RhB reached 70% when the dye solution exposed to visible light for the first 30 min. Further, when the light exposure time increased to 90 min, the degradation ratio increased slowly and achieved 90%.

We also investigate the influence of the pH value of the dye solution on the decolorization efficiency. The experiment was carried out by adjusting the pH of the RhB solution to 3, and the dye and catalyst concentration remaining constant (Fig. 11). It is obvious that a more efficient photodegradation process occurred after adjusting the pH value of the dye solution to 3. When the light application time increases to 15 min, the degradation ratio of RhB has already reaches 92%. The nearly full degradation for RhB in the presence of **2** occurred after another 45 min (with ratio of 95%), resulting in nearly complete decolorization (Figs. 11, Insert and S14). It can also be seen that when no catalyst was added to the system, the degradation of RhB was negligible. These results clearly indicate that the aqueous solution of **2** exhibits high photocatalytic efficiency for the degradation of RhB (especially in acid condition) in the presence of H₂O₂ under visible irradiation. The photocatalytic mechanism may be explained as follows.³⁸⁻³⁹ Under visible light irradiation, valence band and conduction band of **2** generate holes (h⁺) and electrons (e⁻) respectively, both of which can produce hydroxyl radical (HO·) that is known to have high activity to degrade organic dye molecules.⁴⁰

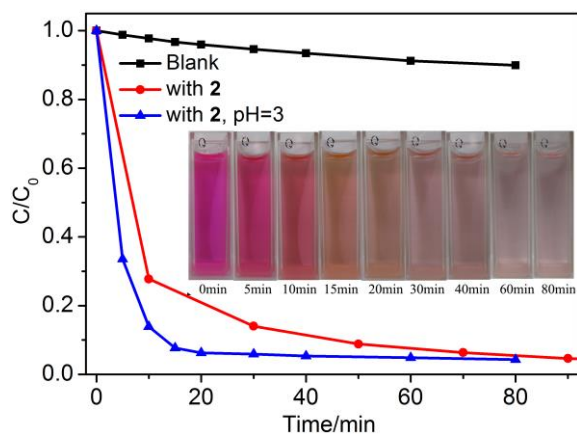


Fig. 11 Time-dependent UV/Vis spectra of dye solutions with or without photocatalyst **2**. Inset: color change photograph image of dye solution with catalyst **2** and pH = 3.

To explore the recyclability of the aqueous solution of **2** as a photocatalyst, recycling experiments of photodegradation activity were performed. As shown in Fig. S15, the aqueous solution of **2** exhibits excellent photocatalytic activity and the degradation ratio was 96% in the first round of illumination.

While, in the fourth and fifth runs, the degradation rate slightly decreased to a mean value of 85%. The recycling test results clearly demonstrate the aqueous solution of **2** can be reused for effective homogeneous photodegradation of RhB under visible light irradiation.

For **1**, similar visible light photocatalytic experiments were also carried out; however no obvious photocatalytic degradation behavior can be observed, which may be due to its negligible absorption of the visible light (Fig. S13).

4. Conclusion

In summary, by utilizing two achiral N,O-coordinated ligands, H₃padc and H₂pidc, to coordinate with Cd(II) or Co(II) ions two MOFs **1** and **2** are obtained, both of which crystallize in polar space groups, and feature intriguing crystal structures with 3-D (4,6)-connected fsc topology for **1** and 2-D (3,6)-connected kgd topology for **2**. Property studies indicate that both **1** and **2** exhibit multiple properties, specifically PL and SHG properties for **1**, antiferromagnetism and visible light photocatalysis properties for **2**. Detailed studies reveal that the PL emission for **1** is mainly originated from the ligand-centered charge transition, and the weak SHG response is ascribed to the presence of SHG-active units that have relative small dipole moments and also are not in complete alignment. While, for **2** the strong antiferromagnetic interaction may mainly occur within the [Co₂] dimer, and the significant absorption in the visible light region may responsible for its effective visible light photocatalytic property. Compounds **1** and **2** may use as multifunctional materials in related areas, and the conclusions obtained in this work will help people a lot in the rational design synthesis of NCS multifunctional MOFs. The preparation of materials with effective SHG response assembled with other property is still in progress in our laboratory.

Acknowledgements

We gratefully acknowledge the financial support by the NSF of China (21201080), the NSF of Shandong Province (ZR2012 BQ011). We are also very grateful to Prof. Dr. G.-C. Guo, Prof. Dr. G. Xu, and Dr. G.-E. Wang at FJIRSM (Fujian Institute of Research on the Structure of Matter, Chinese Academy of Sciences) for their help in SHG measurement and helpful discussions.

Notes and references

^aKey Laboratory of Chemical Sensing & Analysis in Universities of Shandong, School of Chemistry and Chemical Engineering, University of Jinan, Jinan, Shandong 250022, P. R. China

^bSchool of Advanced Materials, Shenzhen Graduate School, Peking University, Shenzhen 518055, P. R. China

E-mail: chm_liugn@ujn.edu.cn (G.-N. Liu), chm_licc@ujn.edu.cn (C. Li).

† Electronic Supplementary Information (ESI) available: Crystallographic data, additional structural figures, TGA curves, IR spectra, and PXRD patterns. CCDC reference number 1407477–1407478 for **1–2**. For ESI and crystallographic data in CIF or other electronic format, see DOI: 10.1039/0000000000

- (a) M. K. Singh, Y. Yang and C. G. Takoudis, *Coord. Chem. Rev.*, 2009, **253**, 2920; (b) D. Maspoch, D. Ruiz-Molina and J. Veciana, *Chem. Soc. Rev.*, 2007, **36**, 770; (c) A. B. Gaspar, V. Ksenofontov, M. Seredyuk and P. Gutlich, *Coord. Chem. Rev.*, 2005, **249**, 2661; (d) C. Train, T. Nuida, R. Gheorghe, M. Gruselle and S. Ohkoshi, *J. Am. Chem. Soc.*, 2009, **131**, 16838; (e) E. Cariati, R. Macchi, D. Roberto, R. Ugo, S. Galli, N. Casati, P. Macchi, A. Sironi, L. Bogani, A. Caneschi and D. Gatteschi, *J. Am. Chem. Soc.*, 2007, **129**, 9410; (f) S. Bernard, P. Yu, T. Coradin, E. Riviere, K. Nakatani and R. Clement, *Adv. Mater.*, 1997, **9**, 981; (g) A. K. Cheetham and C. N. R. Rao, *Science*, 2007, **318**, 58; (h) G. Rogez, N. Viart and M. Drillon, *Angew. Chem., Int. Ed.*, 2010, **49**, 1921; (i) Y. Zhang, W. Q. Liao, D. W. Fu, H. Y. Ye, Z. N. Chen and R. G. Xiong, *J. Am. Chem. Soc.*, 2015, **137**, 4928.
- (a) S. L. Qiu and G. S. Zhu, *Coord. Chem. Rev.*, 2009, **253**, 2891; (b) Y. J. Cui, B. L. Chen and G. D. Qian, *Coord. Chem. Rev.*, 2014, **273**, 76; (c) C. Y. Su and Y. B. Dong, *J. Solid State Chem.*, 2015, **223**, 1; (d) W.-X. Zhang, P.-Q. Liao, R.-B. Lin, Y.-S. Wei, M.-H. Zeng and X.-M. Chen, *Coord. Chem. Rev.*, 2015, **293-294**, 263; (e) X. Q. Liang, F. Zhang, H. X. Zhao, W. Ye, L. S. Long and G. S. Zhu, *Chem. Commun.*, 2014, **50**, 6513; (f) J. Li, J. Yang, Y. Y. Liu and J. F. Ma, *Chem. Eur. J.*, 2015, **21**, 4413; (g) M. Dai, X. R. Su, X. Wang, B. Wu, Z. G. Ren, X. Zhou and J. P. Lang, *Cryst. Growth Des.*, 2014, **14**, 240; (h) J. B. Peng, Q. C. Zhang, X. J. Kong, Y. Z. Zheng, Y. P. Ren, L. S. Long, R. B. Huang, L. S. Zheng and Z. P. Zheng, *J. Am. Chem. Soc.*, 2012, **134**, 3314; (i) X. C. Shan, F. L. Jiang, D. Q. Yuan, H. B. Zhang, M. Y. Wu, L. Chen, J. Wei, S. Q. Zhang, J. Pan and M. C. Hong, *Chem. Sci.*, 2013, **4**, 1484; (j) X. M. Zhang, C. W. Zhao, J. P. Ma, Y. Yu, Q. K. Liu and Y. B. Dong, *Chem. Commun.*, 2015, **51**, 839; (k) x. Wang, L. Zhang, J. Yang, F. Liu, F. Dai, R. Wang and D. Sun, *J. Mater. Chem. A*, 2015, **3**, 12777; (l) S. Yuan, Y. K. Deng and D. Sun, *Chem. Eur. J.*, 2014, **20**, 10093.
- (a) J. E. Mondloch, M. J. Katz, W. C. Isley, P. Ghosh, P. L. Liao, W. Bury, G. Wagner, M. G. Hall, J. B. DeCoste, G. W. Peterson, R. Q. Snurr, C. J. Cramer, J. T. Hupp and O. K. Farha, *Nat. Mater.*, 2015, **14**, 512; (b) R. B. Lin, F. Li, S. Y. Liu, X. L. Qi, J. P. Zhang and X. M. Chen, *Angew. Chem., Int. Ed.*, 2013, **52**, 13429; (c) M. Zhang, M. T. Zhang, C. Hou, Z. F. Ke and T. B. Lu, *Angew. Chem., Int. Ed.*, 2014, **53**, 13042; (d) S. D. Han, J. P. Zhao, S. J. Liu and X. H. Bu, *Coord. Chem. Rev.*, 2015, **289**, 32; (e) Q. P. Lin, X. H. Bu, A. G. Kong, C. Y. Mao, X. Zhao, F. Bu and P. Y. Feng, *J. Am. Chem. Soc.*, 2015, **137**, 2235; (f) J. C. Yu, Y. J. Cui, C. D. Wu, Y. Yang, B. L. Chen and G. D. Qian, *J. Am. Chem. Soc.*, 2015, **137**, 4026; (g) X. Liu, L. Li, Y. Z. Yang and K. L. Huang, *Dalton Trans.*, 2014, **43**, 4086; (h) L. E. Kreno, K. Leong, O. K. Farha, M. Allendorf, R. P. Van Duyne and J. T. Hupp, *Chem. Rev.*, 2012, **112**, 1105; (i) S. S. Nagarkar, B. Joarder, A. K. Chaudhari, S. Mukherjee and S. K. Ghosh, *Angew. Chem., Int. Ed.*, 2013, **52**, 2881; (j) J. Qin, B. Ma, X.-F. Liu, H.-L. Lu, X.-Y. Dong, S.-Q. Zang and H. Hou, *J. Mater. Chem. A*, 2015, **3**, 12690.
- (a) H. Furukawa, F. Gandara, Y. B. Zhang, J. C. Jiang, W. L. Queen, M. R. Hudson and O. M. Yaghi, *J. Am. Chem. Soc.*, 2014, **136**, 4369; (b) M. Dinca and J. R. Long, *Angew. Chem., Int. Ed.*, 2008, **47**, 6766; (c) K. Sumida, D. L. Rogow, J. A. Mason, T. M. McDonald, E. D. Bloch, Z. R. Herm, T. H. Bae and J. R. Long, *Chem. Rev.*, 2012, **112**, 724; (d) M. P. Suh, H. J. Park, T. K. Prasad and D. W. Lim, *Chem. Rev.*, 2012, **112**, 782; (e) H. H. Wu, Q. H. Gong, D. H. Olson and J. Li, *Chem. Rev.*, 2012, **112**, 836; (f) T. F. Liu, D. W. Feng, Y. P. Chen, L. F. Zou, M. Bosch, S. Yuan, Z. W. Wei, S. Fordham, K. C. Wang and H. C. Zhou, *J. Am. Chem. Soc.*, 2015, **137**, 413.
- (a) J. R. Li, J. Sculley and H. C. Zhou, *Chem. Rev.*, 2012, **112**, 869; (b) Q. Chen, Z. Chang, W. C. Song, H. Song, H. B. Song, T. L. Hu and X. H. Bu, *Angew. Chem., Int. Ed.*, 2013, **52**, 11550; (c) T. M. McDonald, J. A. Mason, X. Q. Kong, E. D. Bloch, D. Gygi, A. Dani, V. Crocella, F. Giordano, S. O. Odoh, W. S. Drisdell, B. Vlasisavljevich, A. L. Dzubak, R. Poloni, S. K. Schnell, N. Planas, K. Lee, T. Pascal, L. W. F. Wan, D. Prendergast, J. B. Neaton, B. Smit, J. B. Kortright, L. Gagliardi, S. Bordiga, J. A. Reimer and J. R. Long, *Nature*, 2015, **519**, 303; (d) F. Luo, C. B. Fan, M. B. Luo, X. L. Wu, Y. Zhu, S. Z. Pu, W. Y. Xu and G. C. Guo, *Angew. Chem., Int. Ed.*, 2014, **53**, 9298; (e) M. Du, C. P. Li, M. Chen, Z. W. Ge, X. Wang, L. Wang and C. S. Liu, *J. Am. Chem. Soc.*, 2014, **136**, 10906; (f) F. Luo, J. L. Chen, L. L. Dang, W. N. Zhou, H. L. Lin, J. Q. Li, S. J. Liu and M. B. Luo, *J. Mater. Chem. A*, 2015, **3**, 9616; (g) X. Chen, A. M. Plonka, D. Banerjee, R. Krishna, H. T. Schaefer, S. Ghose, P. K. Thallapally and J. B. Parise, *J. Am. Chem. Soc.*, 2015, **137**, 7007.
- X. Zhao, X. H. Bu, T. Wu, S. T. Zheng, L. Wang and P. Y. Feng, *Nat. Commun.*, 2013, **4**, 2344.
- (a) P. Horcajada, T. Chalati, C. Serre, B. Gillet, C. Sebrie, T. Baati, J. F. Eubank, D. Heurtaux, P. Clayette, C. Kreuz, J. S. Chang, Y. K. Hwang, V. Marsaud, P. N. Bories, L. Cynober, S. Gil, G. Ferey, P. Couvreur and R. Gref, *Nat. Mater.*, 2010, **9**, 172; (b) H. Wang, J. Xu, D. S. Zhang, Q. Chen, R. M. Wen, Z. Chang and X. H. Bu, *Angew. Chem., Int. Ed.*, 2015, **54**, 5966.
- J.-K. Sun, W.-W. Zhang, T. Akita and Q. Xu, *J. Am. Chem. Soc.*, 2015, **137**, 7063.
- (a) V. Safarifard and A. Morsali, *Coord. Chem. Rev.*, 2015, **292**, 1; (b) N. A. Khan and S. H. Jung, *Coord. Chem. Rev.*, 2015, **285**, 11; (c) H. Y. Cho, J. Kim, S. N. Kim and W. S. Ahn, *Microporous Mesoporous Mater.*, 2013, **169**, 180; (d) S. M. F. Vilela, D. Ananias, J. A. Fernandes, P. Silva, A. C. Gomes, N. J. O. Silva, M. O. Rodrigues, J. P. C. Tome, A. A. Valente, P. Ribeiro-Claro, L. D. Carlos, J. Rocha and F. A. A. Paz, *J. Mater. Chem. C*, 2014, **2**, 3311.
- (a) G. Xu, K. Otsubo, T. Yamada, S. Sakaida and H. Kitagawa, *J. Am. Chem. Soc.*, 2013, **135**, 7438; (b) I. Stassen, M. Styles, T. Van Assche, N. Campagnol, J. Fransaer, J. Denayer, J. C. Tan, P. Falcaro, D. De Vos and R. Ameloot, *Chem. Mater.*, 2015, **27**, 1801; (c) L. Pan, Z. H. Ji, X. H. Yi, X. J. Zhu, X. X. Chen, J. Shang, G. Liu and R. W. Li, *Adv. Funct. Mater.*, 2015, **25**, 2677; (d) Y. Qi, S. P. Lin, C. J. Chen, Y. Liu, Z. P. Qiao, X. J. Kuang, Q. Su and H. Y. Chao, *J. Mater. Chem. A*, 2014, **2**, 8849; (e) W. A. Maza, S. R. Ahrenholtz, C. C. Epley, C. S. Day and A. J. Morris, *J. Phys. Chem. C*, 2014, **118**, 14200.
- For recent publications, please see: (a) L. Wang, W. T. Yang, Y. X. Li, Z. G. Xie, W. Zhu and Z. M. Sun, *Chem. Commun.*, 2014, **50**, 11653; (b) W. Xie, S. R. Zhang, D. Y. Du, J. S. Qin, S. J. Bao, J. Li, Z. M. Su, W. W. He, Q. Fu and Y. Q. Lan, *Inorg. Chem.*, 2015, **54**, 3290; (c) C. Y. Sun, X. L. Wang, X. Zhang, C. Qin, P. Li, Z. M. Su, D. X. Zhu, G. G. Shan, K. Z. Shao, H. Wu and J. Li, *Nat. Commun.*, 2013, **4**; (d) H. L. Liu, L. N. Chang, L. Y. Chen and Y. W. Li, *J. Mater. Chem. A*, 2015, **3**, 8028; (e) Y. J. Cui, R. J. Song, J. C. Yu, M. Liu, Z. Q. Wang, C. D. Wu, Y. Yang, Z. Y. Wang, B. L. Chen and G.

- D. Qian, *Adv. Mater.*, 2015, **27**, 1420; (f) Y. Wang, B. Yuan, Y. Y. Xu, X. G. Wang, B. Ding and X. J. Zhao, *Chem. Eur. J.*, 2015, **21**, 2107; (g) X. L. Hao, Y. Y. Ma, H. Y. Zang, Y. H. Wang, Y. G. Li and E. B. Wang, *Chem. Eur. J.*, 2015, **21**, 3778; (h) Y. X. Ye, L. Q. Zhang, Q. F. Peng, G. E. Wang, Y. C. Shen, Z. Y. Li, L. H. Wang, X. L. Ma, Q. H. Chen, Z. J. Zhang and S. C. Xiang, *J. Am. Chem. Soc.*, 2015, **137**, 913.
12. (a) P.-X. Li, M.-S. Wang, M.-J. Zhang, C.-S. Lin, L.-Z. Cai, S.-P. Guo and G.-C. Guo, *Angew. Chem., Int. Ed.*, 2014, **53**, 11529; (b) P. H. Guo, J. L. Liu, J. H. Jia, J. Wang, F. S. Guo, Y. C. Chen, W. Q. Lin, J. D. Leng, D. H. Bao, X. D. Zhang, J. H. Luo and M. L. Tong, *Chem. Eur. J.*, 2013, **19**, 8769; (c) K. K. Bisht, B. Parmar, Y. Rachuri, A. C. Kathalikattil and E. Suresh, *CrystEngComm*, 2015, **17**, 5341.
13. (a) C. Wang, T. Zhang and W. B. Lin, *Chem. Rev.*, 2012, **112**, 1084; (b) J.-S. Guo, G. Xu, X.-M. Jiang, M.-J. Zhang, B.-W. Liu and G.-C. Guo, *Inorg. Chem.*, 2014, **53**, 4278.
14. (a) G.-N. Liu, X.-M. Jiang, M.-F. Wu, G.-E. Wang, G.-C. Guo and J.-S. Huang, *Inorg. Chem.*, 2011, **50**, 5740; (b) G.-N. Liu, G.-C. Guo, F. Chen, S.-H. Wang, J. Sun and J.-S. Huang, *Inorg. Chem.*, 2012, **51**, 472; (c) G.-N. Liu, J.-D. Lin, Z.-N. Xu, Z.-F. Liu, G.-C. Guo and J.-S. Huang, *Cryst. Growth Des.*, 2011, **11**, 3318.
15. W. M. Wendlandt and H. G. Hecht, *Reflectance Spectroscopy*. Interscience: New York, 1966.
16. (a) M. D. Segall, P. J. D. Lindan, M. J. Probert, C. J. Pickard, P. J. Hasnip, S. J. Clark and M. C. Payne, *J. Phys.: Condens. Matter*, 2002, **14**, 2717; (b) V. Milman, B. Winkler, J. A. White, C. J. Pickard, M. C. Payne, E. V. Akhmatkaya and R. H. Nobes, *Int. J. Quantum Chem.*, 2000, **77**, 895.
17. D. R. Hamann, M. Schluter and C. Chiang, *Phys. Rev. Lett.*, 1979, **43**, 1494.
18. Z. Shi, L. Li, S. Niu, J. Jin, Y. Chi, L. Zhang, J. Liu and Y. Xing, *Inorg. Chim. Acta*, 2011, **368**, 101.
19. L. Pan, X. Y. Huang and J. Li, *J. Solid State Chem.*, 2000, **152**, 236.
20. Agilent, *CrysAlisPro*. Version 1.171.35.21 ed.; Agilent Technologies Corp.: California, America.
21. Siemens, *SHELXTL Version 5 Reference manual*. Siemens Energy & Automaion Inc.: Madison, WI, 1994.
22. A. L. Spek, *J. Appl. Crystallogr.*, 2003, **36**, 7.
23. (a) S. Banerjee, A. Ghosh, B. Wu, P. G. Lassahn and C. Janiak, *Polyhedron*, 2005, **24**, 593; (b) S. Banerjee, P. G. Lassahn, C. Janiak and A. Ghosh, *Polyhedron*, 2005, **24**, 2963.
24. (a) B. M. Kukovec, G. A. Venter and C. L. Oliver, *Cryst. Growth Des.*, 2012, **12**, 456; (b) H. Wang, L. H. Huo, Z. P. Deng, H. Zhao and S. Gao, *CrystEngComm*, 2012, **14**, 3501; (c) G. B. Li, J. R. He, M. Pan, H. Y. Deng, J. M. Liu and C. Y. Su, *Dalton Trans.*, 2012, **41**, 4626.
25. (a) K. P. Rao, M. Higuchi, J. G. Duan and S. Kitagawa, *Cryst. Growth Des.*, 2013, **13**, 981; (b) T. Ladrak, S. Smulders, O. Roubeau, S. J. Teat, P. Gamez and J. Reedijk, *Eur. J. Inorg. Chem.*, 2010, 3804; (c) L. Q. Yang, D. C. Crans, S. M. Miller, A. la Cour, O. P. Anderson, P. M. Kaszynski, M. E. Godzala, L. D. Austin and G. R. Willsky, *Inorg. Chem.*, 2002, **41**, 4859.
26. V. A. Blatov, A. P. Shevchenko and V. N. Serezhkin, *J. Appl. Crystallogr.*, 2000, **33**, 1193.
27. (a) N. Sakagami, M. Nakahanada, K. Ino, A. Hioki and S. Kaizaki, *Inorg. Chem.*, 1996, **35**, 683; (b) S. Baitalik, P. Bag, U. Florke and K. Nag, *Inorg. Chim. Acta*, 2004, **357**, 699; (c) S. Baitalik, U. Florke and K. Nag, *Inorg. Chim. Acta*, 2002, **337**, 439; (d) Y. M. Chen, L. N. Zheng, S. X. She, Z. Chen, B. Hu and Y. H. Li, *Dalton Trans.*, 2011, **40**, 4970.
28. Y. Q. Sun, J. Zhang, Y. M. Chen and G. Y. Yang, *Angew. Chem., Int. Ed.*, 2005, **44**, 5814.
29. (a) S. L. Zheng and X. M. Chen, *Aust. J. Chem.*, 2004, **57**, 703; (b) A. Barbieri, G. Accorsi and N. Armaroli, *Chem. Commun.*, 2008, 2185; (c) T. Hirano, K. Kikuchi, Y. Urano and T. Nagano, *J. Am. Chem. Soc.*, 2002, **124**, 6555; (d) J. J. Wang, C. S. Liu, T. L. Hu, Z. Chang, C. Y. Li, L. F. Yan, P. Q. Chen, X. H. Bu, Q. Wu, L. J. Zhao, Z. Wang and X. Z. Zhang, *CrystEngComm*, 2008, **10**, 681.
30. H. Yang, R. L. Sang, X. Xu and L. Xu, *Chem. Commun.*, 2013, **49**, 2909.
31. (a) S. K. Kurtz and T. T. Perry, *J. Appl. Phys.*, 1968, **39**, 3798; (b) M.-J. Zhang, B.-X. Li, B.-W. Liu, Y.-H. Fan, X.-G. Li, H.-Y. Zeng and G.-C. Guo, *Dalton Trans.*, 2013, **42**, 14223.
32. (a) X. Y. Wang, L. Gan, S. W. Zhang and S. Gao, *Inorg. Chem.*, 2004, **43**, 4615; (b) M. Clemente-Leon, E. Coronado, C. Marti-Gastaldo and F. M. Romero, *Chem. Soc. Rev.*, 2011, **40**, 473; (c) A. Rodriguez, R. Kivekas and E. Colacio, *Chem. Commun.*, 2005, 5228; (d) Y. Chen, S. She, Q. Gao, D. Gao, D. Wang, Y. Li, W. Liu and W. Lib, *CrystEngComm*, 2014, **16**, 1091.
33. (a) F. Chen, F.-K. Zheng, G.-N. Liu, A.-Q. Wu, M.-S. Wang, S.-P. Guo, M.-F. Wu, Z.-F. Liu, G.-C. Guo and J.-S. Huang, *Inorg. Chem. Commun.*, 2010, **13**, 278; (b) N. Berg, S. M. Taylor, A. Prescimone, E. K. Brechin and L. F. Jones, *CrystEngComm*, 2012, **14**, 2732.
34. (a) M. Moragues-Canovas, C. E. Talbot-Eeckelaers, L. Catala, F. Lloret, W. Wernsdorfer, E. K. Brechin and T. Mallah, *Inorg. Chem.*, 2006, **45**, 7038; (b) C. Y. Niu, X. F. Zheng, X. S. Wan and C. H. Kou, *Cryst. Growth Des.*, 2011, **11**, 2874.
35. J. G. Hou, C. Yang, Z. Wang, S. Q. Jiao and H. M. Zhu, *Appl. Catal., B*, 2013, **129**, 333.
36. L. Hammarstrom and S. Hammes-Schiffer, *Acc. Chem. Res.*, 2009, **42**, 1859.
37. (a) C. C. Wang, J. R. Li, X. L. Lv, Y. Q. Zhang and G. S. Guo, *Energy Environ. Sci.*, 2014, **7**, 2831; (b) M. Dai, H.-X. Li and J.P. Lang, *CrystEngComm*, 2015, **17**, 4741.
38. T. Wen, D. X. Zhang and J. Zhang, *Inorg. Chem.*, 2013, **52**, 12.
39. (a) Z. Li, L. W. Mi, W. H. Chen, H. W. Hou, C. T. Liu, H. L. Wang, Z. Zheng and C. Y. Shen, *CrystEngComm*, 2012, **14**, 3965; (b) G.-N. Liu, J.-R. Shi, X.-J. Han, X. Zhang, K. Li, J. Li, T. Zhang, Q.-S. Liu, Z.-W. Zhang and C. Li, *Dalton Trans.*, 2015, **44**, 12561; (c) F. Sheng, X. Zhu, W. Wang, H. Bai, J. Liu, P. Wang, R. Zhang, L. Han and J. Mu, *J. Mol. Catal. A: Chem.* 2014, **393**, 232.
40. Now, whether the structure of **2** changed after dissolved in water is unclear. According to the absorption spectra of **2** in solid state and in solution (Fig. S13), which are in basic agreement with each other. The main connections between Co²⁺ and deprotonated H₂picdic ligands may retain. Detailed study is still in progress.